PAPER

Combustion–explosion suppression and environmental protection of typical sulfur-containing hazardous chemicals

Xinrui Zhang,[a] Zhiyue Han, [ID] *[a] Cheng Wang,*[a] Yue Yu[b] and Binbin Wu[a]

Sulfur, as a crucial chemical raw, poses increased combustion–explosion risks when mixed with other hazardous substances due to its dual nature as both an oxidant and a reducing agent. Additionally, sulfur-induced combustion and explosions can result in environmental pollution. Combustion–explosion suppression technology plays a crucial role in industrial production by effectively preventing hazardous chemical explosion incidents. This research investigates the combustion–explosion suppression of black powder, a common hazardous chemical containing sulfur, by utilizing two solid-based blast suppressants, $NH_4H_2PO_4$ and $NaHCO_3$. On this basis, examining changes in the oxidation states of sulfur and explaining the mechanisms of combustion–explosion suppression through the examination of combustion–explosion products. Additionally, numerical calculations are employed to analyze the evolution patterns of gaseous and solid-phase products throughout the entire combustion–explosion process. Research indicates that $NaHCO_3$ exhibits a more effective combustion–explosion suppression effect on black powder compared to $NH_4H_2PO_4$, which attributed to the valence state transformation of sulfur and the reduction of carbon oxidation. Furthermore, with the enhancement of combustion–explosion suppression effect, K_2S, which a pollutes the environment, is gradually transform converted into potassium fertilizer K_2SO_4, which benefits plants. These results offer new insights into the research of combustion–explosion suppression of sulfur-containing substances and environmental protection strategies.

1 Introduction

Sulfur (S) is a crucial chemical raw material with a wide range of applications in various industries, including agriculture, explosives, pharmaceuticals, and food.[1,2] It can ignite when exposed to an open flame, leading to a violent fire that releases toxic gases, leading to environmental pollution, and some scholars have systematically studied the explosion hazard of sulfur dust.[3,4] Additionally, sulfur can act as both an oxidizing and reducing agent due to its multiple valence states. Therefore, when combined with other flammable substances, it can pose a greater risk.[5]

Black powder is a typical hazardous chemical containing sulfur. Due to the addition of sulfur, it has excellent combustion properties. Therefore, to this day it also has various applications such as petroleum drilling, coal mining, explosive shaping, explosion welding, and fireworks.[6,7] Unfortunately, accidents frequently occur in black powder production enterprises during the processes of production, transportation, and storage, resulting in huge property losses, casualties and environmental pollution. There is a pressing need for the development of safe and effective safety measures.

Explosion suppression technology, a method with high potential for reducing or eliminating explosion hazards, is known for its practicality, cost-effectiveness, and safety. It is used to prevent gas and dust explosions in industries such as coal mining, fuel, and metallurgy.[8–11] This technology used in the production of black powder, it is anticipated to effectively address the issue of explosions. The core of explosion suppression technology is explosion suppressants, including CO_2, N_2, $NH_4H_2PO_4$, water, Halon, and so on.[12–17] Gas suppressants that rely on diluted oxygen concentration may have limited effectiveness due to the self-supply of oxygen by black powder. Additionally, the use of Halon will result in the production of toxic and harmful gases during the suppression process, leading to environmental pollution and damage to the ozone layer. At the same time, under low concentration conditions, Halon may even have the unintended effect of promoting combustion.[18,19] Furthermore, the use of water to suppress sulfur-containing substances can result in the production of large quantities of H_2S and sulfuric acid, posing a serious threat to both personnel and the environment present on-site.

[a]State Key Laboratory of Explosion Science and Safety Protection, Beijing Institute of Technology, Beijing, 100081, China. E-mail: hanzhiyue@bit.edu.cn; wangcheng@bit.edu.cn

[b]College of Life Science and Technology, Beijing University of Chemical Technology, Beijing 100029, China

Therefore, solid-based suppressants are a more suitable choice. The two most widely used solid-based suppressants in the field of fire extinguishing are ABC dry powder and BC dry powder. Their main ingredients, $NH_4H_2PO_4$ and $NaHCO_3$, exhibit both physical and chemical explosion suppression effects.[20] Consequently, this work selects these compounds as typical solid suppressants for research.

$NH_4H_2PO_4$ and $NaHCO_3$ have been extensively utilized in research on gas and dust explosions in previous studies. Jiang *et al.* investigated their efficacy in suppressing combustion and explosion of aluminum powder and biomass dust.[21,22] The results indicate that $NH_4H_2PO_4$ exhibits superior performance compared to $NaHCO_3$ in inhibiting aluminum powder combustion, whereas $NaHCO_3$ demonstrates advantages when dealing with biomass dust. Wei *et al.* conducted a study on the suppression of explosions in hydrogen/dimethyl ether/methane/air mixtures using a water mist containing $NaHCO_3$. The research revealed that the addition of $NaHCO_3$ significantly reduced the average flame propagation speed and the maximum explosion pressure of the combustible gases. When $W_{NaHCO_3} = 7\%$ and $\Phi = 1.0$, the decreasing rates of the average flame propagation speed of CH_4-enriched flames, DME-enriched flames and H_2-enriched flames are 84.9%, 29.5% and 40.8%, respectively.[23] Pang *et al.* investigated the inhibitory effect of $NH_4H_2PO_4$ on the flame propagation of aluminum alloy dust clouds. The study unveiled that at a $NH_4H_2PO_4$ median diameter of 10.58 μm and a concentration of 80%, both the distance and speed of the aluminum alloy dust explosion flame reached their minimum values.[24] The studies mentioned above collectively demonstrate the promising blast suppression capabilities of $NH_4H_2PO_4$ and $NaHCO_3$. Applying these substances to the combustion and explosion suppression of black powder holds the potential to address existing challenges effectively.

To sum up, this study examines the combustion–explosion suppression of black powder, a typical S-containing hazardous chemical, using two solid-based blast suppressants, $NH_4H_2PO_4$ and $NaHCO_3$. The study investigates alterations in the oxidation states of sulfur, mechanisms of combustion–explosion suppression through analysis of combustion–explosion products, and the environmental impact of the combustion–explosion suppression process. Furthermore, numerical calculations are utilized to analyze the evolution patterns of gaseous and solid-phase products during the entire combustion–explosion process.

2 Experimental

2.1 Source of raw materials

The purity of all chemicals in this study higher than 98%. They are $NH_4H_2PO_4$, AR, Beijing Tongguang Fine Chemicals Company; $NaHCO_3$, AR, Beijing Tongguang Fine Chemicals Company; KNO_3, AR, Beijing Tongguang Fine Chemicals Company; S, AR, Shandong Xiya Chemical Company Limited; Chinese fir charcoal, can pass 500 mesh sieve, Jiangshan Luyi Bamboo Charcoal Company Limited. $NH_4H_2PO_4$ and $NaHCO_3$ were thoroughly ground, dried, and sieved through the sieve (300 mesh) before the experiment.

2.2 Preparation of black powder

Black powder was prepared with a ratio of $KNO_3 : S : C$ at $75 : 10 : 15$. The KNO_3 and S were thoroughly crushed and dried, and then sifted through a 300 mesh sieve. The resulting powder was carefully mixed with Chinese fir charcoal powder and dried until a constant mass was achieved, resulting in black powder for future use.

The combustion temperature of the prepared black powder was tested by thermocouples according to the previous method in our present work,[25] and the maximum temperature reached approximately 1100 °C, as shown in Fig. 1.

2.3 Combustion–explosion pressure testing experiment

To evaluate the effectiveness of different suppressants in mitigating black powder, a closed experimental platform for explosive testing was designed, which shown in Fig. 2. This platform comprises a 12 V-powered pressure sensor (0–10 MPa), an enclosed explosive device (100 mL), and an oscilloscope (Tektronix DPO4104). The enclosed explosive device has two ends: the sampling end, which is equipped with a pressure sensor, and the excitation end, which has wiring terminals that connect to a powder package. The outermost side of the powder package is aluminum foil. When making powder packets, first flatten the aluminum foil, and then the suppressants are evenly covered on its inner surface. Next, the black powder is stacked on top of the suppressants, making the suppressants uniformly wrapped around the outer layer of the black powder during the experiment. An electric igniter is used to excite the black powder by the battery, and the oscilloscope collects data through the pressure sensor to obtain the p–t curve. Due to the intense combustion–explosion reaction process, each experimental condition was repeated 3–5 times during the experiment.

2.4 Characterization and analysis of combustion–explosion products

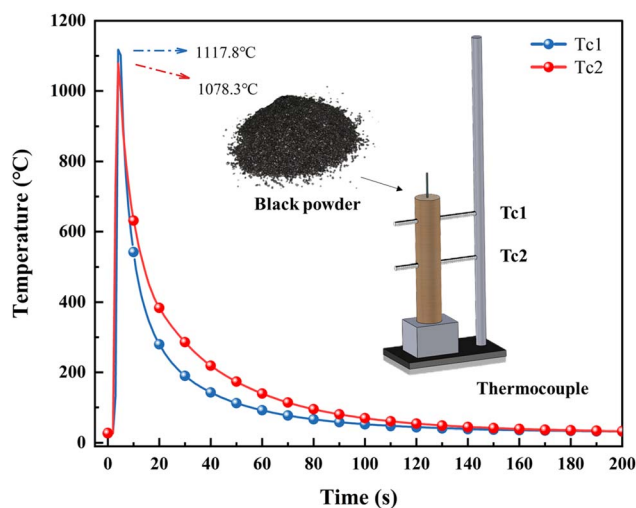To comprehensively understand the changes during the combustion–explosion process, we analyzed pressure change

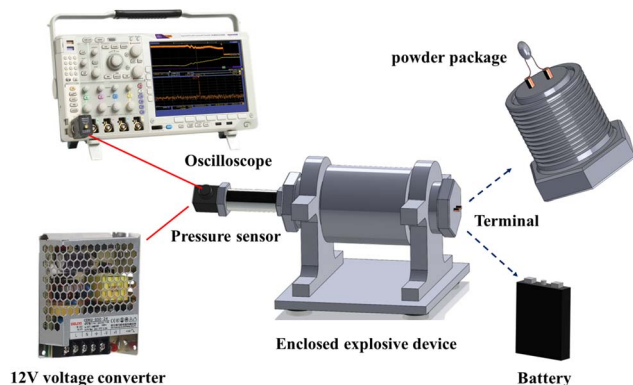**Fig. 1** Test results of combustion temperature of black powder.

Fig. 2 Enclosed explosive experimental platform.

Fig. 3 p–t curve of suppression of black powder under different dosages of $NH_4H_2PO_4$.

data and considered the physical endothermic effects of suppressants, which were obtained from TG-DSC tests. The test conditions for $NH_4H_2PO_4$ were as follows: a temperature ramp of 30–800 °C, with N_2 as the carrier gas and a flow rate of 10 mL min^{-1}, using the Mettler TGA/DSC 1. Since $NaHCO_3$ continues to decompose at temperatures above 800 °C, we employed the Mettler TGA/DSC 3+ to conduct tests at 30–1000 °C, while maintaining the other conditions consistent with those used for $NH_4H_2PO_4$.

To investigate the combustion–explosion suppression mechanism of black powder, we collected explosion products, including both gaseous and solid components. For the analysis of the solid products, XRD (Rigaku SmartLab SE, Japan) was used with a copper target, scanning in the 2θ range of 5° to 90° at a speed of 2° min^{-1}. Additionally, XPS (Thermo Scientific K Alpha, USA) were employed. GC (Aglient 7890B, USA) was utilized to analyze the gaseous products. Subsequently, the results of the product characterization were then used to assess the environmental protection impact of the combustion–explosion suppression process.

2.5 Thermodynamic equilibrium product analysis

Based on the product analysis in 2.4, the equilibrium products of different suppressants and black powder at different temperatures (25–1100 °C) were calculated using the equilibrium composition model in HSC Chemistry 6.0 by Outokumpu Research Oy., which is calculated using the GIBBS solver, with a total of 200 steps. Through the analysis of the changes in equilibrium products, the combustion–explosion suppression mechanisms of $NH_4H_2PO_4$ and $NaHCO_3$ were thoroughly elucidated.

3 Result and discussion

3.1 Result of combustion–explosion pressure testing experiment

3.1.1 Suppression of black powder by $NH_4H_2PO_4$. The suppression effectiveness of $NH_4H_2PO_4$ on black powder was evaluated through the experiment. Different dosages of $NH_4H_2PO_4$ (0.03 g, 0.05 g, 0.07 g, 0.1 g, and 0.15 g) were used on

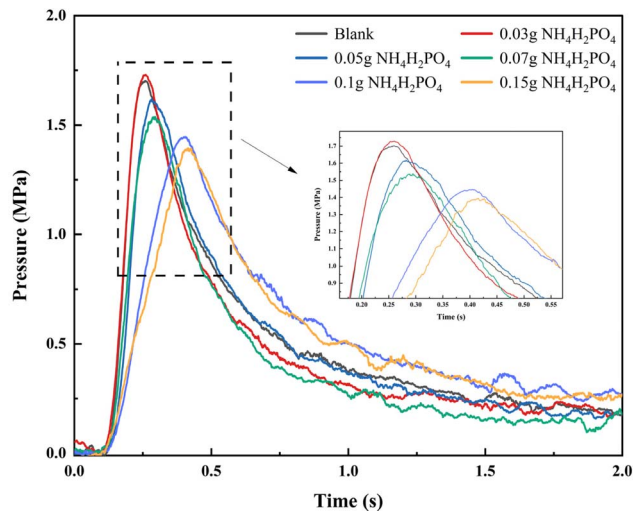1 g of black powder. The results of the p–t curves are presented in Fig. 3.

The p–t curve provides information on the maximum combustion–explosion pressure, time, and rate of black powder under different dosages of $NH_4H_2PO_4$. These results are statistically presented in Fig. 4 and Table 1.

Based on the statistical data analysis, a small amount of $NH_4H_2PO_4$ has a marginal promotional effect on black powder.

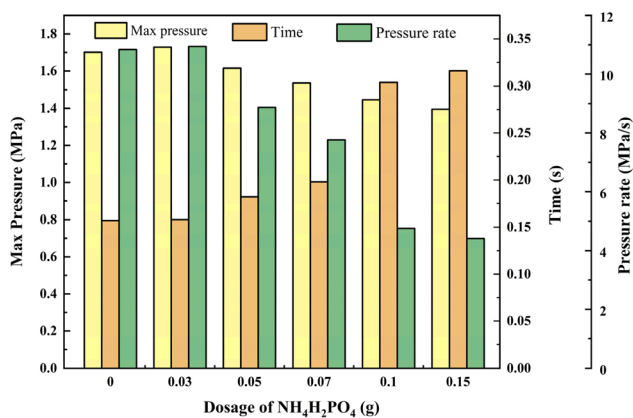Fig. 4 Result from p–t curve in different dosage of $NH_4H_2PO_4$.

Table 1 Result of combustion–explosion suppression experiment in different dosage of $NH_4H_2PO_4$

Dosage of $NH_4H_2PO_4$ (g)	Max pressure (MPa)	Time (s)	Pressure rate (MPa s^{-1})
0 g	1.701	0.157	10.834
0.03 g	1.729	0.158	10.943
0.05 g	1.615	0.182	8.874
0.07 g	1.537	0.198	7.763
0.1 g	1.446	0.304	4.757
0.15 g	1.395	0.316	4.414

When the dosage is 0.03 g, the maximum combustion–explosion pressure increases by 1.64%, and the combustion–explosion rate rises by 1.01%. This effect is attributed to the gaseous products generated by the decomposition of $NH_4H_2PO_4$, a phenomenon defined as the Suppressant Enhanced Explosion Parameter (SEEP). This phenomenon is frequently observed in the explosion suppression processes associated with dust explosions. Many scholars believe that both physical and chemical factors contribute to the occurrence of SEEP, typically resulting in a slight to moderate increase in the maximum explosion pressure and the rate of explosion propagation, which aligns with our experimental findings.[26,27] Notably, the SEEP phenomenon is particularly prevalent when ammonium dihydrogen phosphate is utilized as suppressants, as documented in research concerning explosion prevention and control involving materials such as Al, Mg, and nano Ti.[28,29]

As the dosages of the suppressant gradually increases, the suppressive action of $NH_4H_2PO_4$ becomes progressively stronger. At the dosages of 0.05 g, 0.07 g, 0.1 g and 0.15 g, the maximum combustion–explosion pressure decreased by 5.06%, 9.64%, 14.99% and 17.99%, respectively, and the combustion–explosion pressure rise rate decreased by 18.09%, 28.35%, 56.09% and 59.26%. At the same time, the suppressant had a prolonged effect on the combustion–explosion pressure rise time, adding 0.15 g of $NH_4H_2PO_4$ extended the time by 101.27%.

Consistent with Section 3.1.1, different dosages of $NaHCO_3$ (0.03 g, 0.05 g, 0.07 g, 0.1 g, and 0.15 g) were used on 1 g of black powder, and the $p–t$ curves are presented in Fig. 5.

3.1.2 Suppression of black powder by $NaHCO_3$. Fig. 6 and Table 2 present the maximum combustion–explosion pressure, time, and rise rate of black powder with varying types of suppressants.

Statistical data reveals that the suppressive effects of $NaHCO_3$ on the combustion–explosion behavior of black powder differ from those of $NH_4H_2PO_4$. The combustion–explosion pressure consistently decreases as the $NaHCO_3$

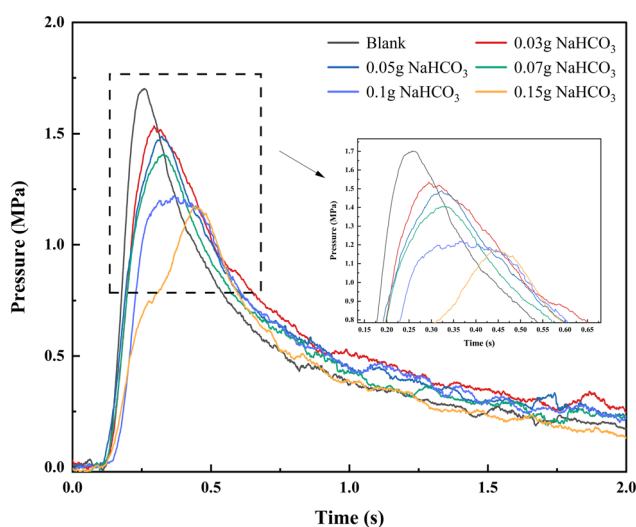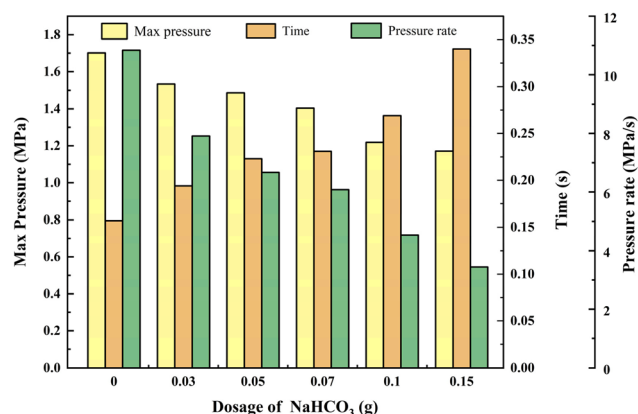Fig. 6 Result from $p–t$ curve in different dosage of $NaHCO_3$.

Table 2 Result of combustion–explosion suppression experiment in different dosage of $NaHCO_3$

Dosage of $NaHCO_3$	Max pressure (MPa)	Time (s)	Pressure rate (MPa s^{-1})
Blank	1.701	0.157	10.834
0.03 g	1.535	0.194	7.912
0.05 g	1.487	0.223	6.668
0.07 g	1.404	0.231	6.078
0.1 g	1.219	0.269	4.532
0.15 g	1.171	0.34	3.444

dosage increases, and there is no promotion phenomenon observed at lower dosages. When different amounts of suppressants were used (0.03 g, 0.05 g, 0.07 g, 0.1 g, and 0.15 g), the maximum combustion–explosion pressure of black powder decreased by 9.76%, 12.58%, 17.46%, 28.33%, and 31.16% respectively, and the combustion–explosion rise rate also decreased by 26.97%, 38.45%, 43.90%, 58.17%, and 68.21%. Consistent with $NH_4H_2PO_4$, $NaHCO_3$ also significantly prolonged the combustion–explosion time, with 0.15 g of $NaHCO_3$ extending the combustion–explosion time by 116.56%.

3.1.3 Calculation of completely suppressed dosage. Based on the experimental data, it can be inferred that the maximum combustion–explosion pressure of black powder suppresses a decreasing trend with the addition of suppressants (after exceeding 0.03 g). However, it should be noted that when the suppressants addition surpasses 0.15 g in the experiment, a substantial amount of residues is produced. Therefore, to further analyze the anticipated changes in the pressure trend, SPSS 27 was employed to fit the data for maximum combustion–explosion pressure, and the results are shown in Fig. 7.

The fitting result of $NH_4H_2PO_4$ is shown in Fig. 7(a) ($R^2 = 0.960$). Based on the fitting curve, the dosage at which the $NH_4H_2PO_4$ completely suppresses the pressure drop to 0 is defined as 0.783 g. Similarly, the fitting result of $NaHCO_3$ is shown in Fig. 7(b) ($R^2 = 0.983$). The corresponding completely suppressed dosage for $NaHCO_3$ is found to be 0.369 g.

To verify the effectiveness of the fitting, 0.79 g and 0.37 g of $NN_4H_2PO_4$ and $NaHCO_3$ were mixed with 1 g of black powder

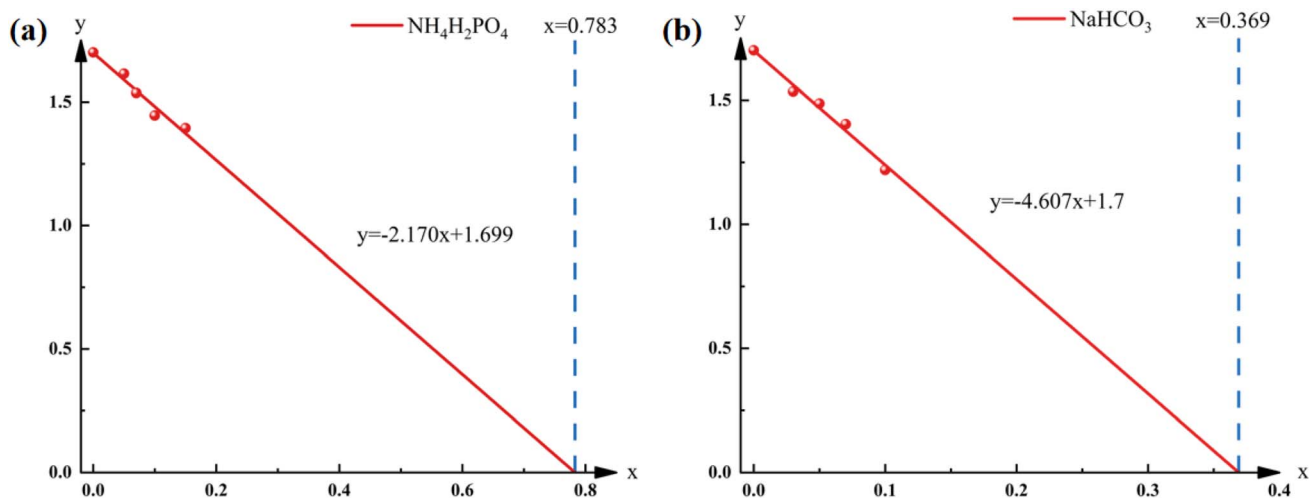Fig. 5 $p–t$ curve of suppression of black powder under different dosage of $NaHCO_3$.

Fig. 7 The fitting results of different suppressants. (a) $NH_4H_2PO_4$ and (b) $NaHCO_3$.

respectively to simulate the conditions under complete reaction. It was found that even with the use of an electric ignition device with high-energy ignition powder, the black powder couldn't be fully ignited, indicating the reliability of the fitting results.
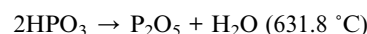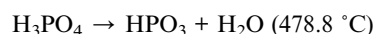
Based on the above data, it can be concluded that for the black powder system, $NaHCO_3$ showed a more significant suppressive effect compared to $NH_4H_2PO_4$. According to the complete suppressed dose analysis, the required suppressive dosage for $NH_4H_2PO_4$ is 2.12 times that of $NaHCO_3$. Additionally, at the same suppressant dosage, the maximum combustion–explosion pressure and combustion–explosion rise rate for $NaHCO_3$ are significantly lower than those for $NH_4H_2PO_4$.

3.2 Analysis of combustion–explosion products

3.2.1 Heat absorption during the combustion–explosion suppression process. Both $NH_4H_2PO_4$ and $NaHCO_3$ suppress physical and chemical suppressant effects. They absorb heat and decompose in high-temperature explosion fields, serving

a physical cooling function. The TG-DSC characterization of these compounds is illustrated in Fig. 8.

The $NH_4H_2PO_4$ powder decomposition process consists of the following reactions:

$$NH_4H_2PO_4 \rightarrow H_3PO_4 + NH_3 \ (211.3 \ ^{\circ}C)$$

$$H_3PO_4 \rightarrow HPO_3 + H_2O \ (478.8 \ ^{\circ}C)$$

$$2HPO_3 \rightarrow P_2O_5 + H_2O \ (631.8 \ ^{\circ}C)$$

There is one obvious endothermic peak in the DSC curve at the temperature around 211.3 °C. The heat absorbed by the rapid decomposition of the $NH_4H_2PO_4$ into NH_3 and H_3PO_4 is $-52.99 \ J \ g^{-1}$.

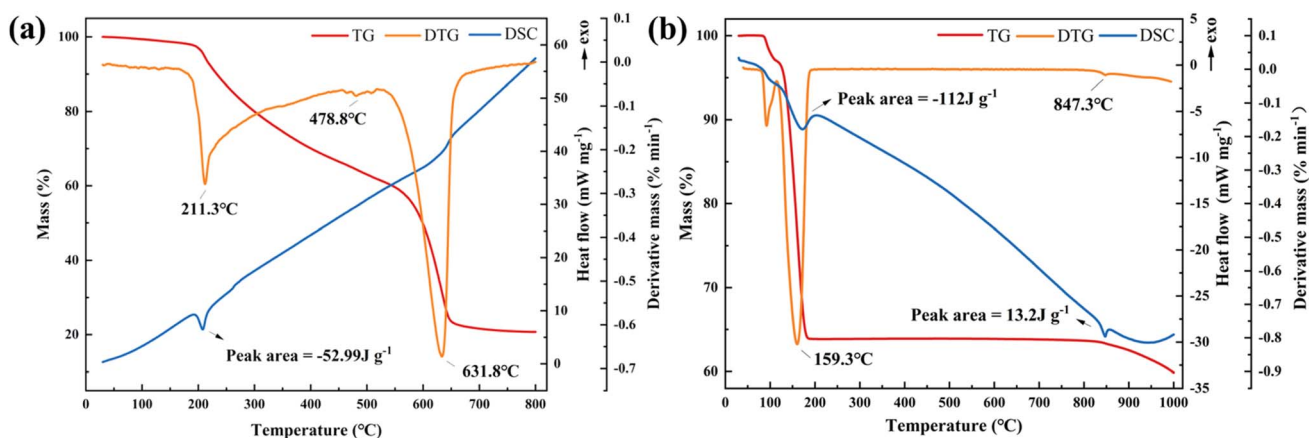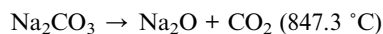The $NaHCO_3$ powder decomposition process consists of the following reactions:

$$NaHCO_3 \rightarrow Na_2CO_3 + H_2O \ (159.3 \ ^{\circ}C)$$

Fig. 8 The TG-DSC results of different suppressants. (a) $NH_4H_2PO_4$ and (b) $NaHCO_3$.

$$Na_2CO_3 \rightarrow Na_2O + CO_2 \ (847.3 \ °C)$$

The DSC curve exhibited two prominent endothermic peaks at approximately 159.3 °C and 847.3 °C. The heat absorbed during rapid decomposition was measured at -112 J g^{-1} and -13.2 J g^{-1}, respectively.

In summary, the endothermic heat generated by the decomposition of the suppressants is significantly smaller than the heat emitted during the combustion of black powder.[30–32] Therefore, it is evident that the primary effects of $NH_4H_2PO_4$ and $NaHCO_3$ in suppressing combustion and explosion arise from chemical reactions that are closely related to their combustion and explosion products.

3.2.2 Analysis of combustion–explosion product. To comprehensively understand the transformation of black powder components during the suppression of combustion–explosion process, solid-phase products were collected before and after suppression and analyzed using XRD. The results revealing that black powder transforms into K_2SO_4 and K_2S after the combustion–explosion. $NH_4H_2PO_4$ reacts with black powder in the combustion–explosion field, leading to the formation of KH_2PO_4 and KPO_3, and $NaHCO_3$ evolves into Na_2SO_4 and $Na_3H(CO_3)_2$ (a mixture of $NaHCO_3$ and Na_2CO_3), which shown in Fig. 9 and 10. Notably, the suppression product of $NaHCO_3$ exhibited the presence of K_2CO_3 and $KHCO_3$ components, attributed primarily to the higher reactivity of K in comparison to Na.

In order to investigate the changes of functional groups in $NN_4H_2PO_4$ and $NaHCO_3$, the combustion–explosion products were tested by XPS, with the results as shown in Fig. 11.

Fig. 11(a) presents the full-scan spectrum of the products, revealing a composition mainly consisting of K, C, O, and S. The addition of $NH_4H_2PO_4$, characteristic peaks of P 2p at around 134 eV emerged, indicating the presence of two oxidation states of PO_4^{3-} and PO_3^{-} (KH_2PO_4 and KPO_3), as depicted in Fig. 11(b).
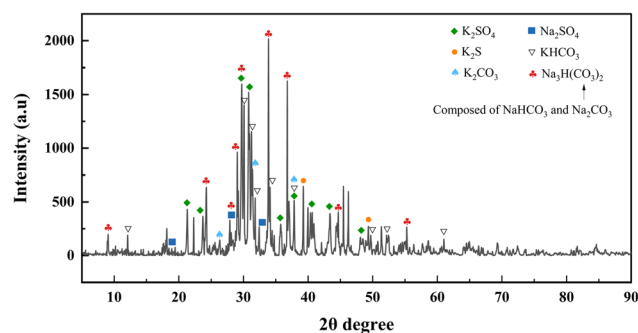

Fig. 10 The XRD characterization results of the products by black powder with $NaHCO_3$.

Meanwhile, the addition of $NaHCO_3$ resulted in the appearance of a distinctive peak of Na 1s at approximately 1071 eV, along with a prominent Auger peak at around 497 eV. Due to the valence state of Na in Na-containing products being +1, it can only exhibit a large characteristic peak, as depicted in Fig. 11(c).

In the overall combustion–explosion reaction, sulfur (S) plays a crucial role. The XRD results indicate that sulfur can act both as an oxidant, producing K_2S, and as a reducing agent, yielding K_2SO_4. To further investigate the binding states of the S element, spectral scanning and Gaussian fitting were conducted, as shown in Fig. 12.

In Fig. 12(a–c), the spin–orbit split peaks ($p_{1/2}$ and $p_{3/2}$) resulting from the presence of S element can be observed, further subdivided into three sub-peaks. The peak corresponding to a binding energy around 162.5 eV is attributed to S^{2-}, while the peak around 168.5 eV corresponds to SO_4^{2-}. Moreover, between the aforementioned peaks, around 166 eV, a minor cross-state S^n (approximately 5% in content, ranging from -2 to $+6$ oxidation states) is still detected. Based on its binding energy, it is likely that this corresponds to SO_3^{2-}.

By calculating the peak areas corresponding to each oxidation state, the proportions of different oxidation states can be
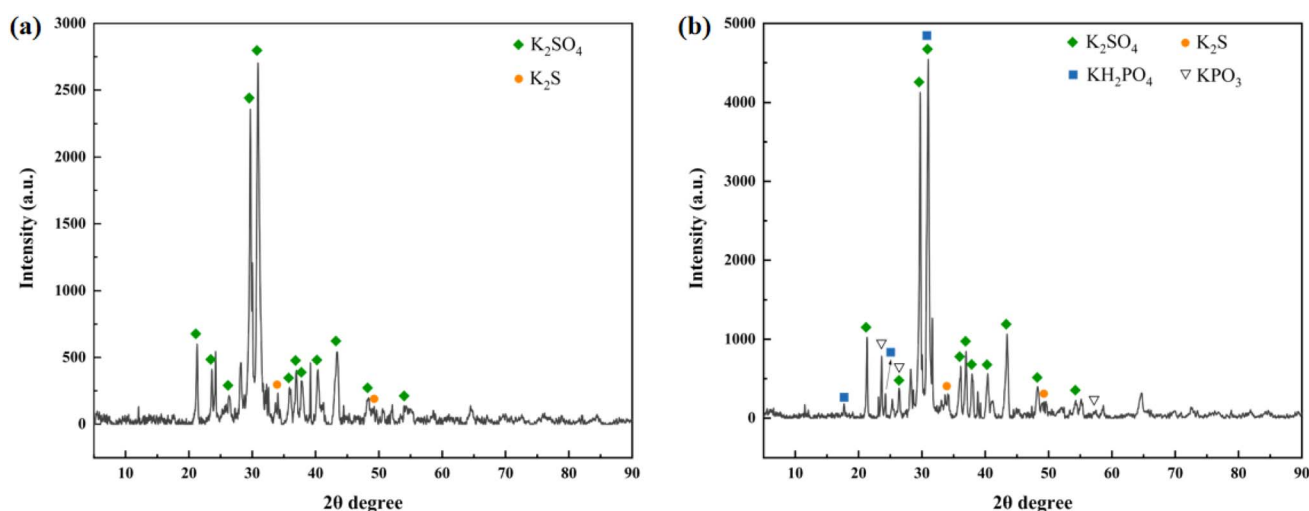

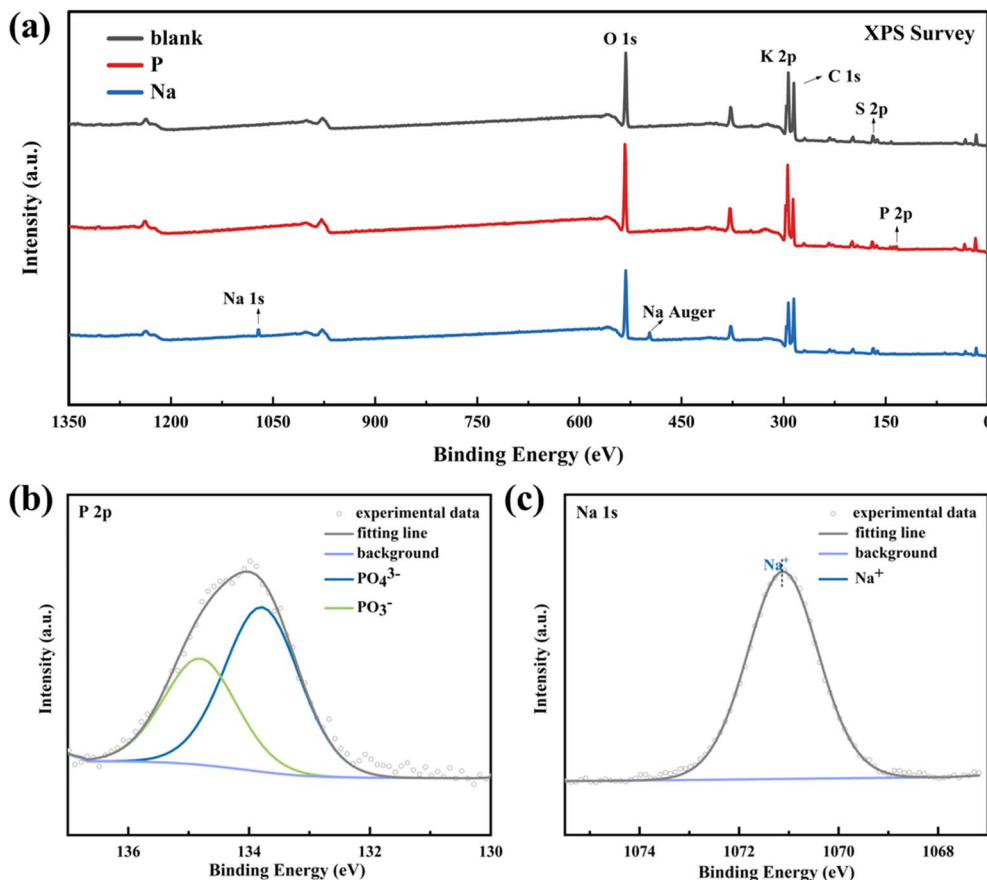Fig. 9 The XRD characterization results of the products (a) blank; (b) black powder with $NH_4H_2PO_4$.

Fig. 11 The XPS characterization results of the combustion–explosion products (a) XPS survey; (b) P 2p peak from black powder with $NH_4H_2PO_4$; (c) Na 1s peak from black powder with $NaHCO_3$.

determined. Comparing the proportions of S^{2-}, S^n, and SO_4^{2-} substances based on their elemental compositions reveals that with increasing strength of suppression (Na > P > Blank), the proportions of S^{2-} and intermediate state S^n gradually decrease, while the proportion of SO_4^{2-} gradually increases, as illustrated in Fig. 12(d). For instance, in the products suppressed by $NaHCO_3$, the content of S^{2-} (K_2S) decreased by 10.93%, while the content of SO_4^{2-} (K_2SO_4) increased by 12.27%. This highlights the transformation of sulfur from being reduced to oxidized during the reaction process, leading to changes in the oxidation states of S, which is crucial in affecting combustion–explosion suppression effectiveness.

Apart from solid-phase products, gas-phase products after combustion–explosion were analyzed using GC, as shown in Fig. 13. It can be observed that the generation of CO_2 and CO decreases after adding suppressants, indicating a decrease in the amount of Chinese fir charcoal powder during the combustion–explosion process, which is consistent with suppression process. Additionally, the content of N_2 in the combustion–explosion products increases significantly with the addition of $NH_4H_2PO_4$, attributed to the introduction of N elements.

3.2.3 Analysis of environmental protection. Through the analysis of combustion–explosion products, it has been noted that as combustion–explosion suppression effect improves,

the presence of K_2S in solid products decreases gradually, while the content of K_2SO_4 increases. According to the Material Safety Data Sheet (MSDS), K_2S, a highly toxic substance, poses a significant threat to aquatic organisms due to its reaction with water. The introduction of K_2S into soil or air can result in substantial environmental harm and the release of toxic gases like H_2S. On the other hand, K_2SO_4 functions as a potent potassium fertilizer, promoting plant growth effectively. Moreover, other byproducts generated during the combustion–explosion suppression process, including KPO_3, KH_2PO_4, K_2CO_3, Na_2CO_3 from $NH_4H_2PO_4$ and $NaHCO_3$, can all serve as plant fertilizers, which are environmentally friendly.

The analysis of gaseous products shows that combustion–explosion suppression effectively reduces both CO_2 and CO, gases known for their environmental hazards. Among them, CO_2 exacerbates the greenhouse effect, while CO, when combined with human hemoglobin, poses significant toxicity. As known from our research, when 0.1 g of $NaHCO_3$ was used, the CO_2 content in the gas product decreased by 7% and the CO content decreased by 13%. The content of CO_2 and CO is expected to further decrease with the enhancement of combustion–explosion suppression efficiency.

Therefore, it can be concluded that using $NH_4H_2PO_4$ and $NaHCO_3$ for black powder suppression not only effectively
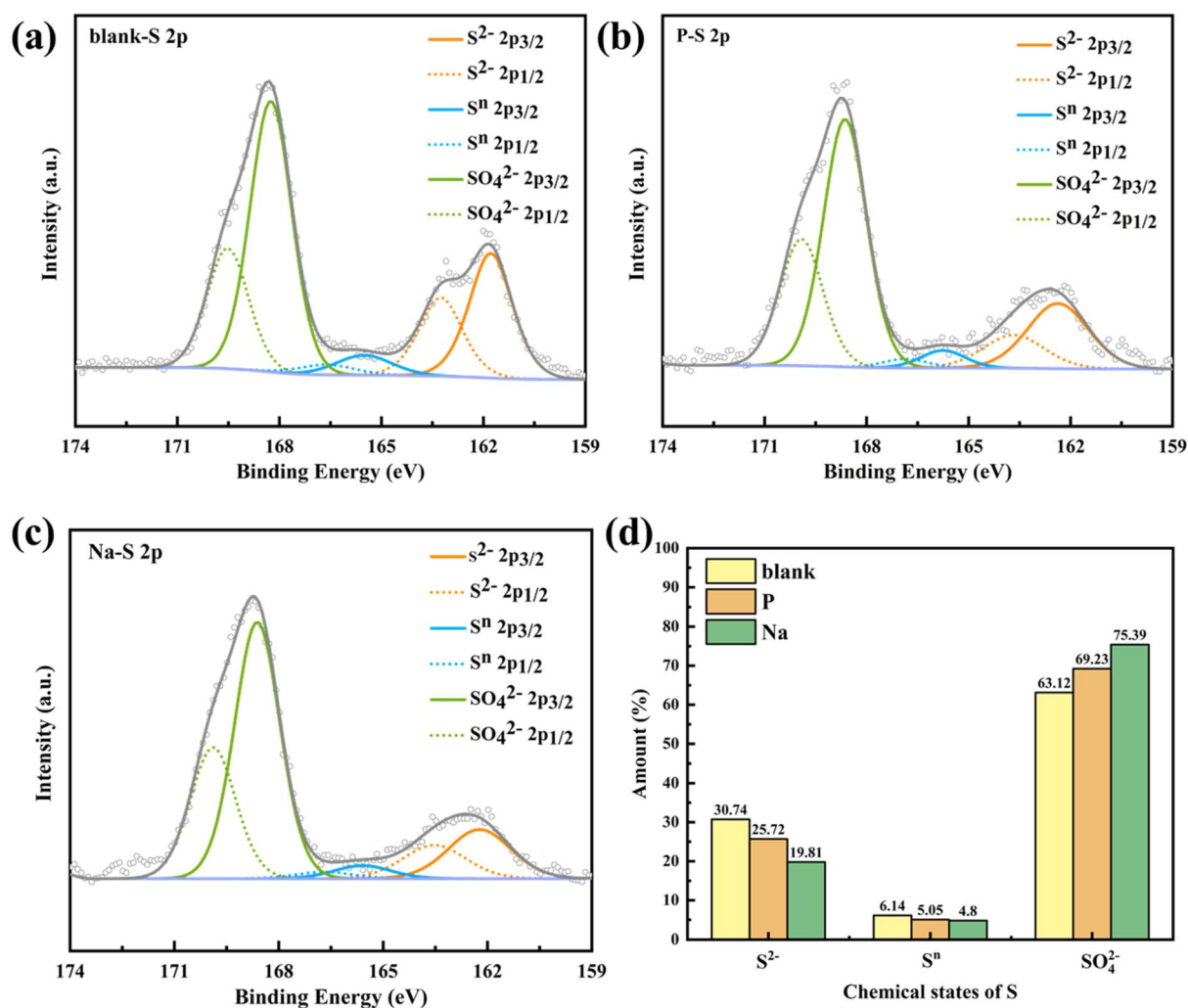
Fig. 12 The XPS characterization results of the combustion–explosion products of S element (a) blank; (b) black powder with $NH_4H_2PO_4$; (c) black powder with $NaHCO_3$; (d) proportional distribution.
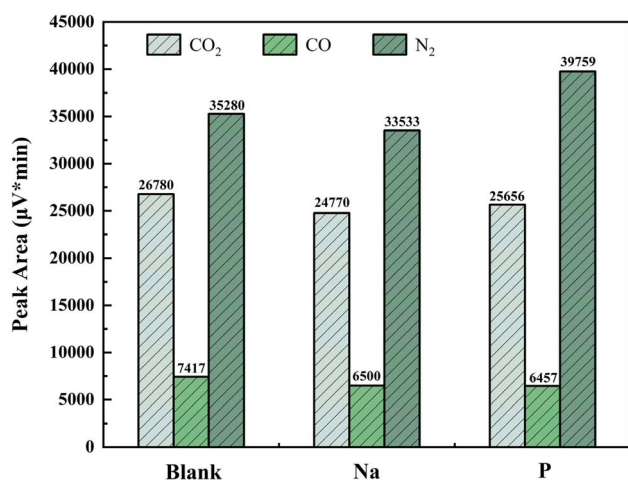

Fig. 13 The GC result of gas-phase product.

reduces the risks associated with combustion–explosion suppression but also helps significantly in reducing the environmental impact of combustion–explosion products.

3.3 Analysis of thermodynamic equilibrium product

To further analyze the evolution process of the combustion–explosion reaction, the research results in Section 3.2 were utilized to simulate the thermodynamic equilibrium products of black powder combustion–explosion with $NH_4H_2PO_4$ and $NaHCO_3$ using the equilibrium composition model in HSC Chemistry.

To enhance the clarity of the simulation results, the experiment's pharmaceutical equivalent was scaled up from mol to kmol and calculated based on the actual proportions. The calculation outcomes are depicted in Fig. 14 and 15.

The variation of gaseous products with temperature is illustrated in Fig. 14(a). In addition to CO_2 and CO produced during the combustion–explosion of black powder, the decomposition of $NH_4H_2PO_4$ also gradually yields H_2O and a small amount of NH_3. With increasing temperature, NH_3 breaks down into N_2 and H_2, which is consistent with the decomposition pattern observed in TG-DSC analysis. Fig. 14(b) shows the variation of solid-phase products. It can be seen that the derivative product KH_2PO_4, formed from $NH_4H_2PO_4$,
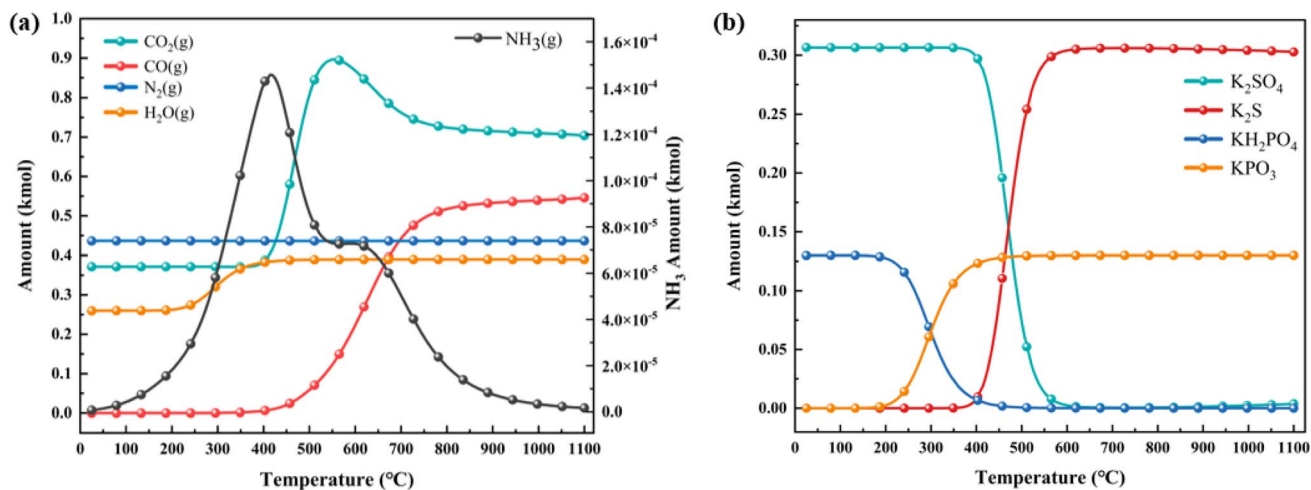
Fig. 14 Simulation results of thermodynamic equilibrium products containing $NH_4H_2PO_4$ (a) gas-phase products; (b) solid-phase products.

undergoes secondary decomposition at high temperatures, resulting in the formation of KPO_3, in line with the characterization results of the products.

The computational results of gaseous products shown in Fig. 15(a) exhibit similarities to those in Fig. 14(a). Water vapor present in the products is a byproduct of the decomposition of $NaHCO_3$. Within the solid-phase products, gradual decomposition of $KHCO_3$ and $NaHCO_3$ occurs as temperature increases, leading to the formation of $NaHCO_3$, K_2CO_3, and small quantities of Na_2SO_4. At temperatures nearing 600 °C, there is a possibility of secondary decomposition of K_2CO_3. Nevertheless, since no analogous derivative compounds were detected during product characterization, further exploration of this phenomenon is not pursued.

Upon observing both figures simultaneously, it becomes evident that at temperatures reaching up to 1100 °C during the full combustion of black powder, S will all converted into K_2S. This observation is consistent with the reaction equation of black powder.

$$2KNO_3 + S + 3C = K_2S + N_2 + 3CO_2$$
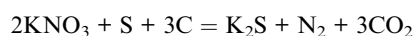
However, at lower reaction temperatures, K_2SO_4 is primarily formed initially. Only when the temperature reaches 400 °C does a notable conversion from K_2SO_4 to K_2S occur. This observation is consistent with the alteration in the S oxidation state as determined by XPS analysis. The presence of suppressants in black powder induces a physical endothermic effect that decreases the reaction temperature, causing the chemical reaction to favor the lower temperature range. Consequently, sulfur, intended for reduction to produce K_2S, undergoes oxidation to produce K_2SO_4, resulting in a decrease in combustion–explosion pressure. From this, if the combustion–explosion suppression process can effectively control the reaction temperature below 300 °C, it may prevent the formation of the highly toxic sulfide K_2S. This could lead to the complete conversion of sulfur into the beneficial K_2SO_4 for plant growth, thereby contributing significantly to environmental protection.
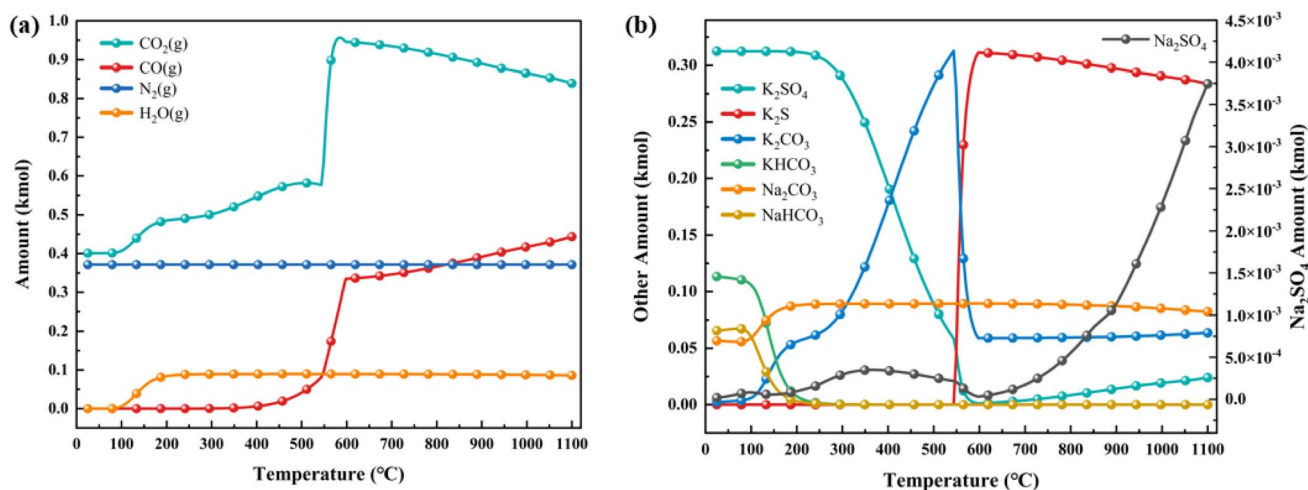

Fig. 15 Simulation results of thermodynamic equilibrium products containing $NaHCO_3$ (a) gas-phase products; (b) solid-phase products.

The variations in gas products suggest that at lower reaction temperatures, the production of CO_2 and CO increases gradually with rising reaction temperature. However, when the reaction temperature surpasses 500 °C, there is a notable increase in the production of CO_2 and CO, consistent with the results observed in gas chromatography. Thus, mitigating the combustion–explosion risks of these substances hinge on early application of suppressants, lowering the reaction temperature, decreasing the involvement of sulfur as an oxidant, and minimizing carbon oxidation.

4 Conclusion

This research examines the combustion–explosion suppression and environmental protection of a typical S-containing hazardous chemical, black powder, using two suppressants, $NH_4H_2PO_4$ and $NaHCO_3$. The conclusions are summarized as follows.

(1) When compared to $NH_4H_2PO_4$, $NaHCO_3$ demonstrates a more pronounced suppression effect on combustion–explosion in black powder. Utilizing a dosage of 0.1 g, $NaHCO_3$ can decrease the maximum combustion–explosion pressure by 28.33%, whereas $NH_4H_2PO_4$ achieves a reduction of only 14.99%. The fitted curves indicate that complete suppression of 1 g of black powder necessitates the addition of 0.783 g of $NH_4H_2PO_4$, while only 0.369 g of $NaHCO_3$ is required.

(2) The combustion–explosion suppression effect of the two suppressants primarily arises from chemical reactions rather than heat absorption. XRD analysis of the combustion–explosion products reveals that $NH_4H_2PO_4$ primarily forms KPO_3 and KH_2PO_4 in the combustion–explosion field, while $NaHCO_3$ mainly produces Na_2SO_4, $KHCO_3$, K_2CO_3, and $Na_3H(CO_3)_2$.

(3) Further analysis of the combustion–explosion products using XPS and GC reveals that as combustion–explosion suppression increases, the toxic K_2S is converted into K_2SO_4, which is beneficial to plants. In the gaseous products, the amounts of CO_2 and CO decrease as combustion–explosion suppression strengthens, leading to positive effects on environmental protection.

(4) The simulation calculation results align with the chemical characterization findings, indicating that effective suppression of these substances relies on early application of suppressants, reducing the reaction temperature, minimizing the involvement of sulfur as an oxidant and reducing charcoal oxidation.

Data availability

Date will be made available on the reader's request.

Conflicts of interest

There are no conflicts to declare.

Acknowledgements

References

1 J. M. Altwal, T. Olewski and L. N. Véchot, Development of a model for the prediction of the ignition properties of combustible dusts undergoing homogeneous combustion: Application to sulfur dust, *Process Saf. Environ. Prot.*, 2022, **168**, 526–534.

2 R. Yao, H. Hu, S. Deng, *et al.*, Structure and saccharification of rice straw pretreated with sulfur trioxide micro-thermal explosion collaborative dilutes alkali, *Bioresour. Technol.*, 2011, **102**(10), 6340–6343.

3 P. Li, M. Li, Z. Liu, *et al.*, Effect of high temperature and sulfur vapor on the flammability limit of hydrogen sulfide, *J. Cleaner Prod.*, 2022, **337**, 130579.

4 K. Sun, Y. Yan, J. Jiang, *et al.*, SO_3 Removal Efficiency and Ash Particle Flowability of Low-Low-Temperature Flue Gas Systems (LLTSs), *Appl. Therm. Eng.*, 2020, **171**(1999), 115132.

5 H. Yan, B. Nie, C. Peng, *et al.*, Evaluation on explosion characteristics and parameters of pulverized coal for low-quality coal: experimental study and analysis, *Environ. Sci. Pollut. Res.*, 2022, 1–17.

6 M. L. Hobbs and M. J. Kaneshige, Cookoff of black powder and smokeless powder, *Propellants, Explos., Pyrotech.*, 2021, **46**(3), 484–493.

7 Y. Sun, Z. Han, Z. Du, *et al.*, Preparation and performance of environmental friendly Sulphur-Free propellant for fireworks, *Appl. Therm. Eng.*, 2017, **126**, 987–996.

8 S. Xu, J. Wang, H. Wang, *et al.*, Hazard evaluation of explosion venting behaviors for aluminum powder/air fuels using experimental and numerical approach, *Powder Technol.*, 2020, **364**, 78–87.

9 K. Yang, Y. Chen, Q. Xiao, *et al.*, Influence of venting coefficient on disastrous effects of aluminium powder explosions, *Process Saf. Environ. Prot.*, 2021, **156**, 72–88.

10 P. Yang, X. Meng, Y. Zhang, *et al.*, Experimental study and mechanism analysis on the suppression of flour explosion by NaCl and $NaHCO_3$, *Combust. Sci. Technol.*, 2023, **195**(16), 4053–4068.

11 D. Qiu, X. Chen, L. Hao, *et al.*, Partial suppression of acetaminophen dust explosion by synergistic multiphase inhibitors, *Process Saf. Environ. Prot.*, 2023, **172**, 262–272.

12 Z. Luo, B. Su, T. Wang, *et al.*, Research progress on explosion control technology and materials of mining gas, *J. Saf. Sci. Technol.*, 2019, **15**(02), 17–24.

13 S. Zhang, X. Wen, Z. Guo, *et al.*, Experimental study on the multi-level suppression of N_2 and CO_2 on hydrogen-air explosion, *Process Saf. Environ. Prot.*, 2023, **169**, 970–981.

14 Q. Zhao, Y. Li, X. Chen, *et al.*, Fire extinguishing and explosion suppression characteristics of explosion suppression system with N$_2$/APP after methane/coal dust explosion, *Energy*, 2022, **257**, 124767.

15 D. X. Du, X. Shen, F. Li, *et al.*, Efficiency characterization of fire extinguishing compound superfine powder containing Mg(OH)$_2$, *J. Loss Prev. Process Ind.*, 2019, **57**, 73–80.

16 B. Liu, Y. Zhang, Y. Zhang, *et al.*, Study on resource utilization of composite powder suppressor prepared from acrylic fiber waste sludge, *J. Cleaner Prod.*, 2021, **291**(1), 125914.

17 X. Wang, Y. Zhang, B. Liu, *et al.*, Effectiveness and mechanism of carbamide/fly ash cenosphere with bilayer spherical shell structure as explosion suppressant of coal dust, *J. Hazard. Mater.*, 2019, **365**, 555e64.

18 J. L. Pagliaro, G. T. Linteris, P. B. Sunderland, *et al.*, Combustion inhibition and enhancement of premixed methane–air flames by halon replacements, *Combust. Flame*, 2015, **162**(1), 41–49.

19 Z. Han, X. Zhang, Y. Yu, *et al.*, *Experimental Investigation of Fire Extinguishing of a Full-Size Battery Box with FK-5-1-12*, Fire Technology, 2022, pp. 1–14.

20 S. Yuan, C. Chang, S. Yan, *et al.*, A review of fire-extinguishing agent on suppressing lithium-ion batteries fire, *J. Energy Chem.*, 2021, **62**, 262–280.

21 H. Jiang, M. Bi, B. Li, *et al.*, Flame inhibition of aluminum dust explosion by NaHCO$_3$ and NH$_4$H$_2$PO$_4$, *Combust. Flame*, 2019, **200**, 97–114.

22 H. Jiang, M. Bi, Q. Peng, *et al.*, Suppression of pulverized biomass dust explosion by NaHCO$_3$ and NH$_4$H$_2$PO$_4$, *Renewable Energy*, 2020, **147**, 2046–2055.

23 S. Wei, M. Yu, B. Pei, *et al.*, Experimental and numerical study on the explosion suppression of hydrogen/dimethyl ether/methane/air mixtures by water mist containing NaHCO$_3$, *Fuel*, 2022, **328**, 125235.

24 L. Pang, H. Peng, S. Sun, *et al.*, Inhibition effect of NH$_4$H$_2$PO$_4$ on explosion flame propagation of aluminum alloy dust cloud, *J. Loss Prev. Process Ind.*, 2023, **85**, 105155.

25 Z. Han, L. Gong, S. Yan, *et al.*, A novel of spacecraft flexible compartment safe and stable inflatable expansion system with the environmental-friendly fuel, *J. Cleaner Prod.*, 2021, **279**, 123843.

26 P. R. Amyotte, Solid inertants and their use in dust explosion prevention and mitigation, *J. Loss Prev. Process Ind.*, 2006, **19**(2–3), 161–173.

27 T. Abbasi and S. A. Abbasi, Dust explosions–Cases, causes, consequences, and control, *J. Hazard. Mater.*, 2007, **140**(1–2), 7–44.

28 Y. Bu, P. Amyotte, C. Li, *et al.*, Effects of dust dispersibility on the suppressant enhanced explosion parameter (SEEP) in flame propagation of Al dust clouds, *J. Hazard. Mater.*, 2021, **404**, 124119.

29 F. Meng, X. Hou, P. Amyotte, *et al.*, Effects of physical and chemical factors on the suppressant enhanced explosion parameter (SEEP) in flame propagation of metal dust layers, *Fuel*, 2023, **334**, 126620.

30 J. Hao, Z. Du, T. Zhang, *et al.*, Influence of NH$_4$H$_2$PO$_4$ powder on the laminar burning velocity of premixed CH$_4$/Air flames, *Int. J. Hydrogen Energy*, 2022, **47**(90), 38477–38493.

31 Y. Li, X. Tian, Y. Ma, *et al.*, Thermal Interaction Mechanisms of Black Powders with Different Particle Sizes and Cellulose as Packing Material during Ignition, *Acta Armamentarii*, 2024, **45**(5), 1582.

32 X. Zhang, Z. Han, C. Wang, *et al.*, Suppression of black powder combustion and explosion using novel green seawater microcapsules, *J. Therm. Anal. Calorim.*, 2024, 1–12.